Electronic Supplementary Material (ESI) for Journal of Materials Chemistry A.

Supplementary Information

Porous Perovskite Calcium-Manganese Oxide Microspheres as Efficient Catalyst for Rechargeable Sodium-Oxygen Batteries

Yuxiang Hu, Xiaopeng Han, Qing Zhao, Jin Du, Fangyi Cheng and Jun Chen*

Key Laboratory of Advanced Energy Materials Chemistry (Ministry of Education) and Collaborative Innovation Center of Chemical Science and Engineering, Nankai University, Tianjin 300071, China

* E-mail address: chenabc@nankai.edu.cn

Experimental Section

Materials Synthesis.

The preparation of $CaMnO_3$ micropheres were synthesized by firing the precursor $CaMn(CO_3)_2$.[s1,s2] Firstly, fresh $MnCO_3$ and $CaCO_3$ were precipitated from $Mn(NO_3)_2$ and $Ca(NO_3)_2$ solution separately with a large excess of $(NH_4)_2CO_3$ and NH_4HCO_3. The carbonate species were washed with distilled water and dried in vacuum overnight. Then, the obtained fresh $MnCO_3$ (1 mmol) and $CaCO_3$ (1 mmol) were dissolved in 10.5 ml 0.5 M dilute nitric acid. After completely dissolving, 20 mL 0.25 M $(NH_4)_2CO_3$ (mole ratio of $CO_3^{2-}/(Ca^{2+}+Mn^{2+})$ = 2.5:1) aqueous solution was added with stirring for 30 min to obtain $CaMn(CO_3)_2$ at room temperature. The precipitate was centrifuged, washed, vacuum-dried overnight. The final $CaMnO_3$ black oxide was obtained by annealing at 900 in air for 5 h. The size of the microspheres would be altered by different experimental reaction temperature (0 ºC and 50 ºC) and mole ratio of CO_3^{2-} precipitant to total cations (Ca^{2+} and Mn^{2+}) (5:1 and 10:1).

Material characterization.

Powder X-ray diffraction (XRD) measurement for the material was performed on a MiniFlex600 X-ray generator (Copper Kα radiation) from 10 to 80° with a step rate of 0.02° and a preset time of 2 s at room temperature. Scanning electron microscopy (SEM) images were collected on a JEOL JSM-7500F microscope (accelerating voltage 5 KV) equipped with energy dispersive spectroscopy (EDS). Transmission electron microscopy (TEM) images for the cathode material were obtained on Philips Tecnai F20 (accelerating voltage 200 KV). The Raman spectroscopies were taken on a confocal Raman microscope (DXR, Thermo-Fisher Scientic) with 532 nm excitation from an argon-ion laser. The specific surface area was analyzed by nitrogen gas adsorption-desorption measurement at 77 K on BELSORP-Mini (Japan). For detecting the electrodes at different discharge/charge states, the electrodes were sealed by the self-made gas-tight sample holder.

Cells Assembly and Electrochemical Tests.

The electrochemical properties of rechargeable $Na–O_2$ cells were tested by CR-2032 type coin cells in this study. For the $CaMnO_3$/C cathode, the slurry of $CaMnO_3$, Super P and poly(vinylidene fluoride) (PVdF) in weight ratio of 30: 60: 10, was mixed in a *N*-methyl-2-pyrrolidone (NMP)

solvent and smeared onto a circular nickel foam. As for the Super P cathode, Super P was mixed with PVdF with the weight ratio of 90:10. Then the mixture was added into NMP solvent and then smeared on the nickel foam with diameter of ~12 mm. The catalyst-afforded nickel foams were vacuum-dried at 110 °C for 6 h. The separator was a glass fiber and sodium served as the anode. 1.0 M sodium triflate salt ($NaSO_3CF_3$) in tetraethylene glycol dimethyl ether (TEGDME) was used as the electrolyte. All the rechargeable Na−O_2 batteries were assembled in an argon-filled glove box (Mikrouna). The batteries were transferred to a sealed container pumped with high-purity oxygen. Cyclic voltammograms (CVs) were conducted on Parstat 263A electrochemical workstation (AMETEK) with a voltage sweep of 0.1 mV s^{-1} from 1.6 V to 3.9 V vs. Na^+/Na. Electrochemical tests of the cells were carried out with a LAND-CT2001A Battery-testing instrument.

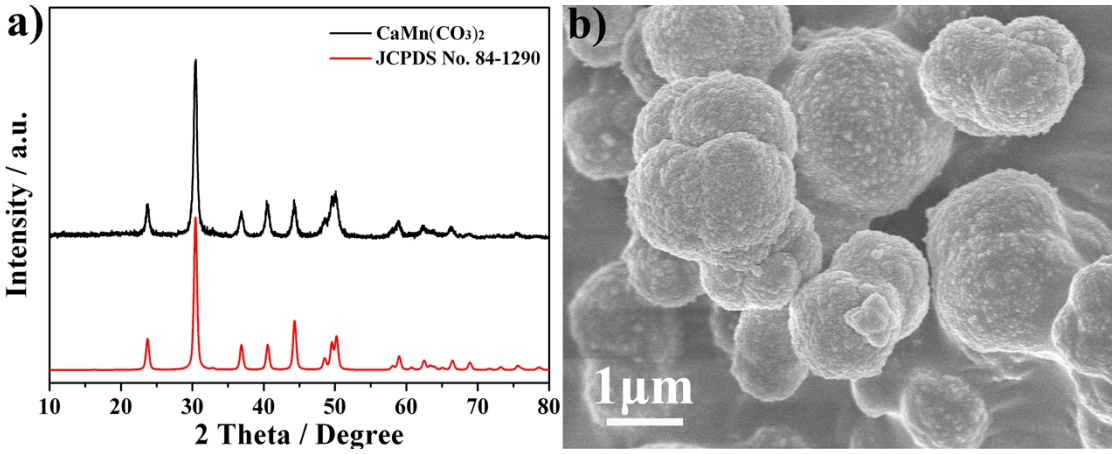

Fig. S1. (a) XRD pattern and (b) SEM image of the carbonate precursor $CaMn(CO_3)_2$.

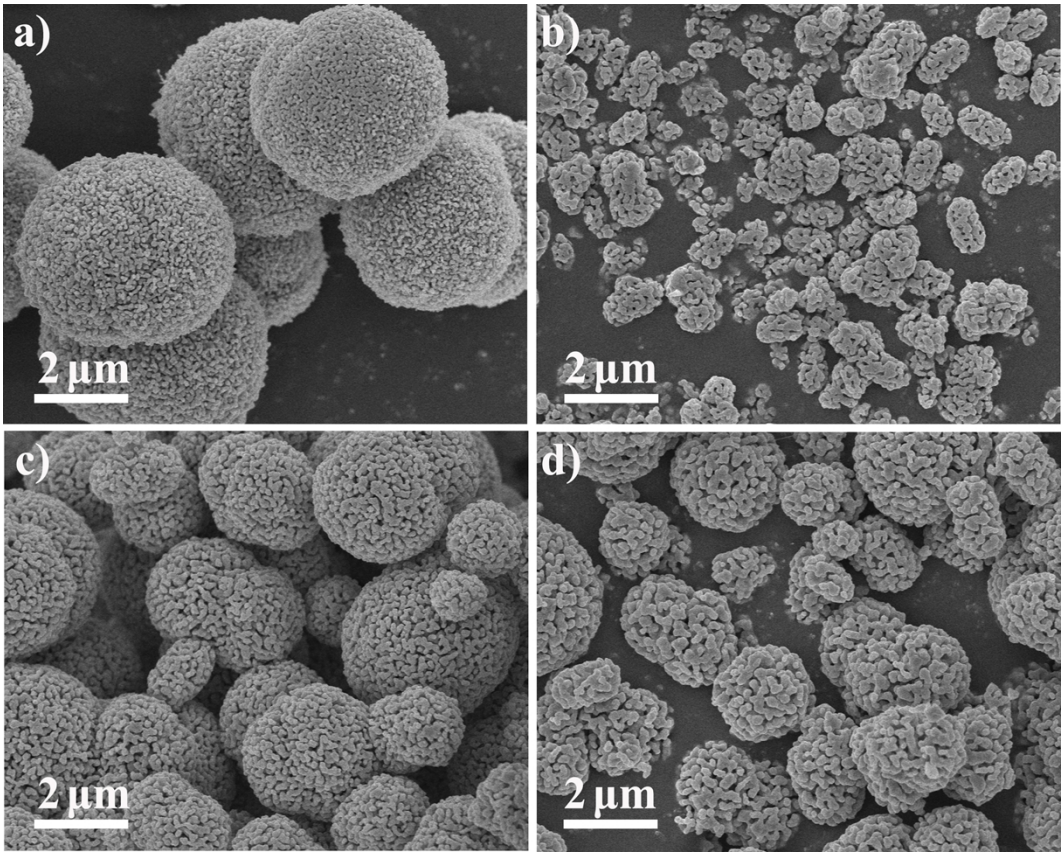

Fig. S2. SEM images of the $CaMnO_3$ microspheres obtained at reaction temperature of 0 ºC (a), 50 ºC (b) and different amount carbonate precipitant with mole ratio of $CO_3^{2-}/(Ca^{2+}+Mn^{2+})$ = 5:1 (c) and 10:1 (d). The high temperature would accelerate the reaction rate and the nucleation instantly completes, resulting in smaller size of the microspheres. Compared with the production at room temperature (2.0-3.0 μm in diameter), the smaller microspheres were obtained at higher temperature of 50 ºC (~ 1.0 μm in diameter) while larger ones were collected at lower temperature of 0 ºC (~ 5.0 μm in diameter). Furthermore, the supersaturation (mole ratio of the CO_3^{2-} / $(Ca^{2+}+Mn^{2+})$) would promote the nucleation rate, leading to the decrease of the microspheres size. Thus we obtained small size of microspheres with increasing ratio of CO_3^{2-} / $(Ca^{2+}+Mn^{2+})$.

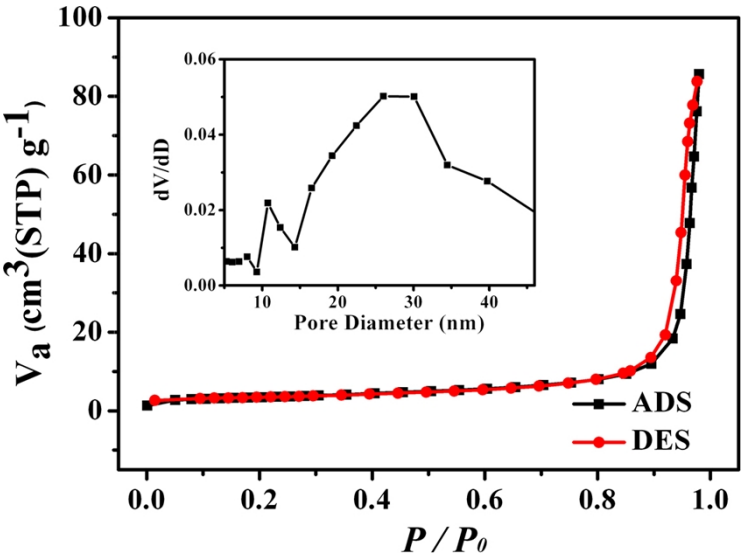

Fig. S3 Nitrogen adsorption-desorption isotherms at 77 K for $CaMnO_3$ microspheres. BET specific surface area is 11.8 m^2 g^{-1}.The inset displays the pore size distribution calculated from desorption isotherm data, showing the main diameter around 30 nm.

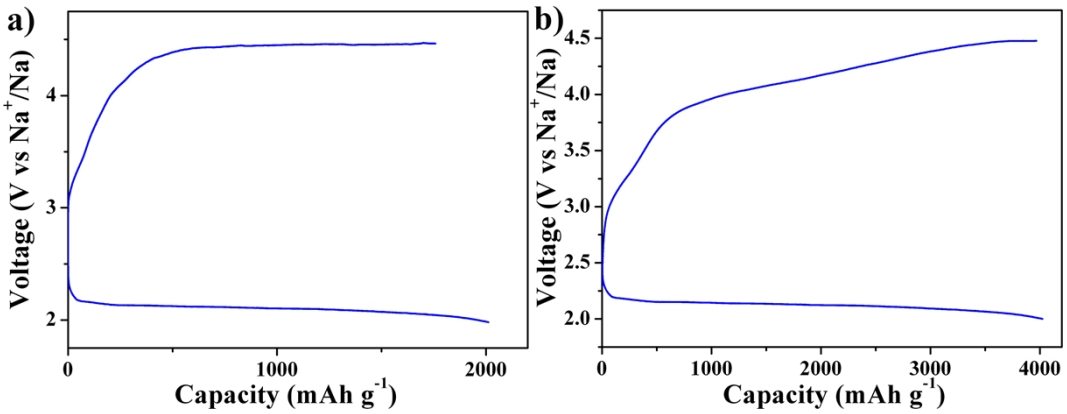

Fig. S4 Charging-discharging curves of (a) Super P and (b) $CaMnO_3$/C using the electrolyte of 1.0 M $NaClO_4$ in propylene carbonate (PC).

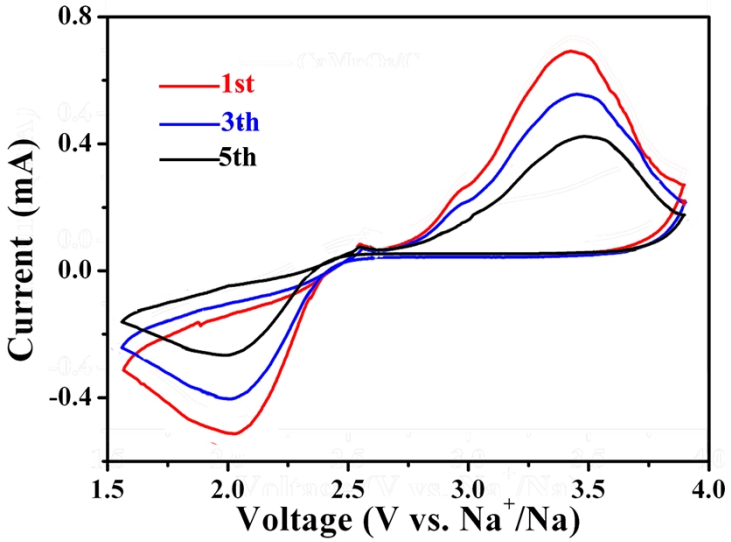

Fig. S5 CV curves of $CaMnO_3$/C electrodes in $NaSO_3CF_3$/TEGDME electrolyte at a scan rate of 0.1 mV s^{-1}. Compared with the pristine cycle, there was no obvious difference of cathodic and anodic peaks positions, indicating the similar redox processes. The slightly lower currents in the later cycles may be ascribed to the possible side reaction and the disposition of the productions that blocking the reaction sites and gas channels.

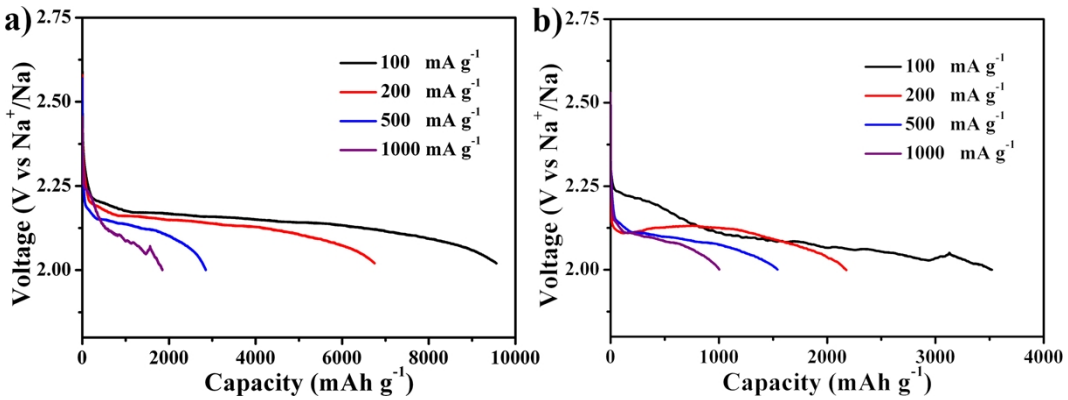

Fig. S6 Rate performance of $CaMnO_3$/C (a) and Super P (b) electrodes.

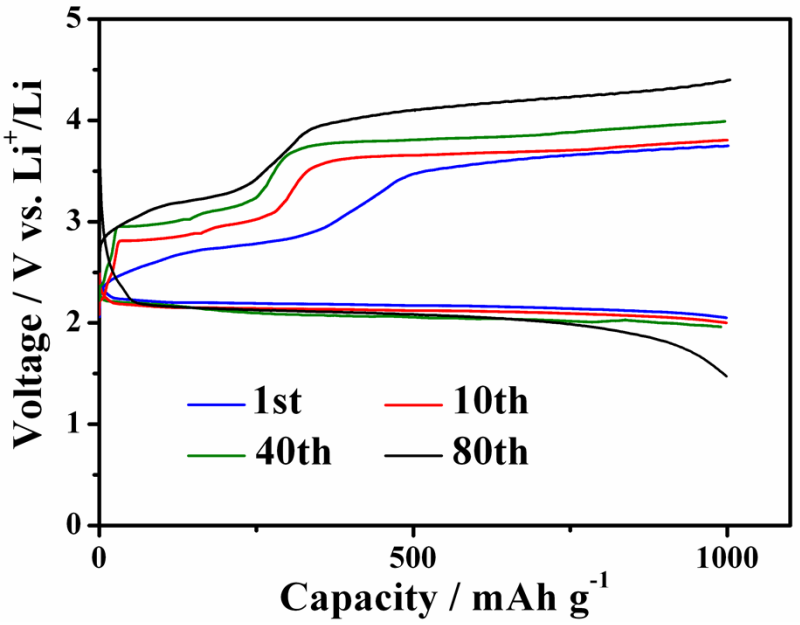

Fig. S7 Discharge–charge curves of the rechargeable Na–O_2 batteries with $CaMnO_3$/C cathode catalysts at selected cycles at a current density of 200 $mA \cdot g^{-1}$ with controlling cycling capacity of 1000 $mAh \cdot g^{-1}$.

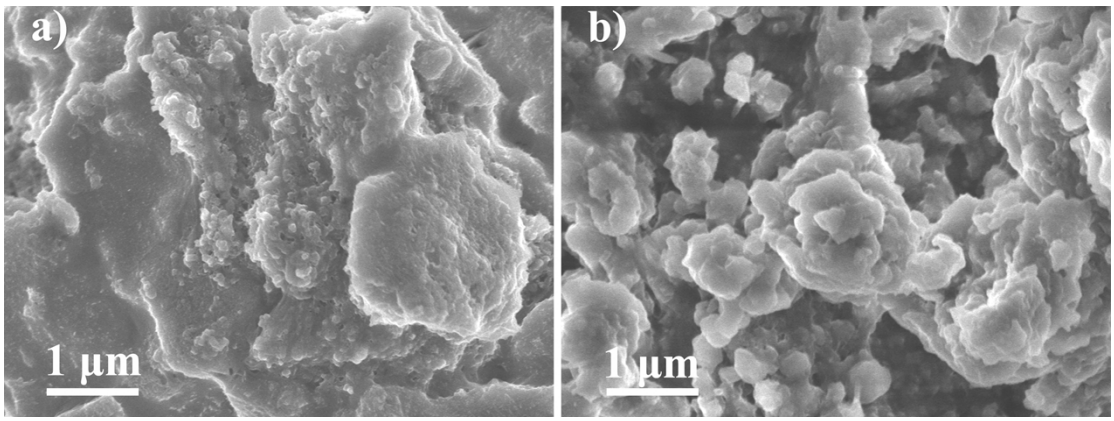

Fig. S8 SEM images of the $CaMnO_3$/C electrode (a) after 80th discharged and (b) after 80th recharged. The insoluble discharge productions precipitate on the surface of the cathode after 80th discharged. However, the cathode does not completely recover to the pristine state with the initial loose and porous morphology after 80th charged. As a result, partial reaction sites and gas channels are blocked, which would lead to decayed performance of battery.

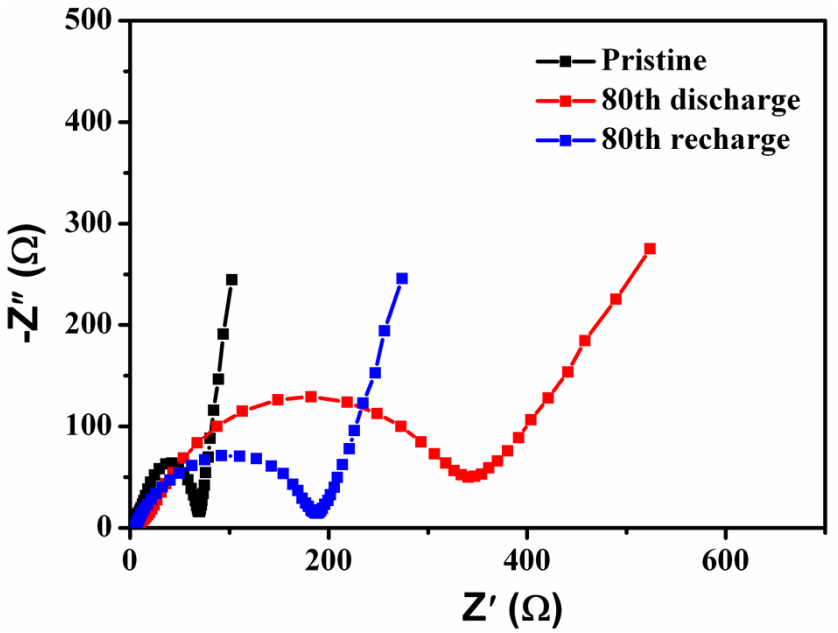

Fig. S9 Electrochemical impedance spectroscopy **(**EIS) results of $CaMnO_3$/C pristine, after 80th discharge and after 80th recharge. The $CaMnO_3$/C-based battery shows little charge transfer resistance (R_{ct}) at the pristine state (70 Ω). Then the resistance of the $CaMnO_3$/C-based batteries would increase to 340 Ω at the end of the 80th discharging. After 80th recharged, the resistance of the $CaMnO_3$/C-based batteries can recover to 190 Ω, which indicates that the cathode cannot completely recover to the pristine state. The increased unrecovered resistance after 80th cycle is an important reason to the decayed performance of the battery.

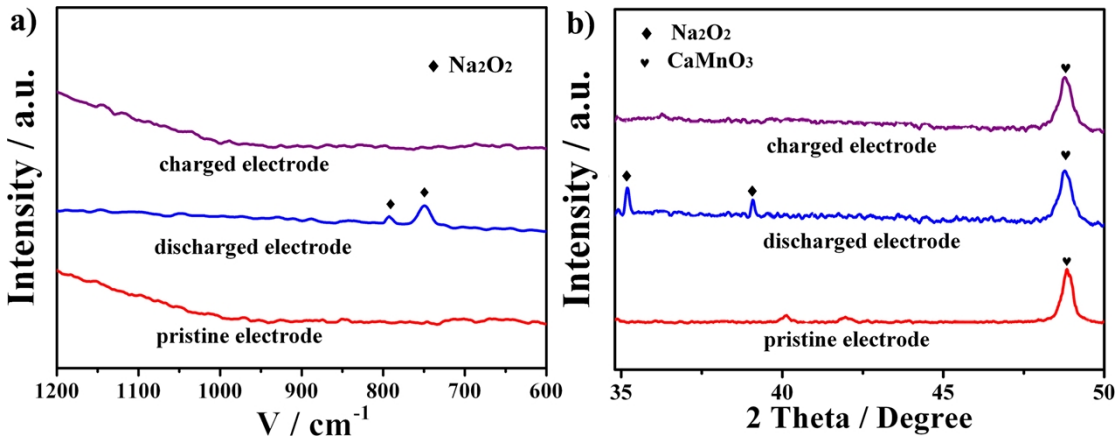

Fig. S10 (a) Raman spectra and (b) XRD patterns of the electrodes at three selected stages in the first cycle with the carbonate-based (propylene carbonate PC) electrolyte: the pristine state, discharging to 2.0 V, and charging to 4.5 V.

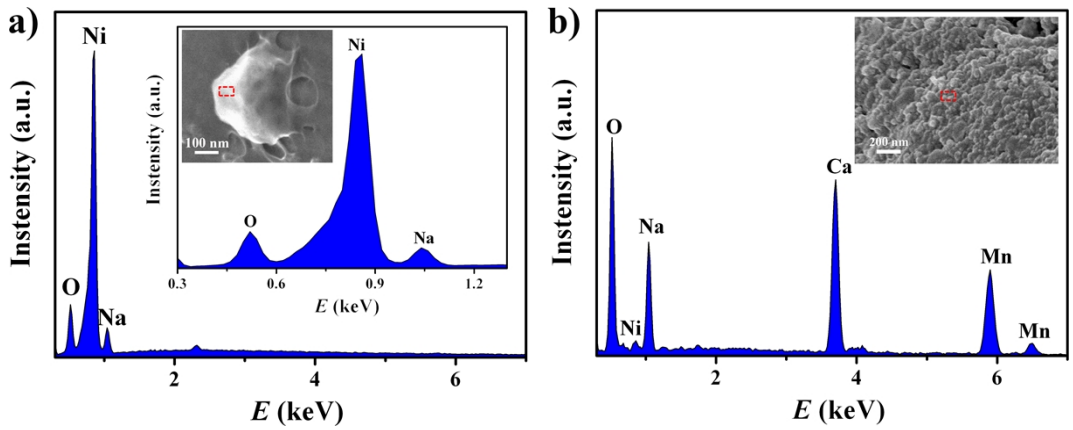

Fig. S11 (a) Energy-dispersive spectroscopy (EDS) spectra of the cubic-like product on the discharged electrode. The inset shows the characteristic element signals, SEM image and the corresponding area of EDS measurement. (b) EDS spectra in other position on the discharged electrode. The inset shows the SEM image and the location of the EDS measurement. The characterization signals collected from the cubic-like species are related to oxygen, sodium and nickel elements with a relative atomic composition of about 26%, 13% and 60%, respectively, which offer further evidence of the existence of NaO_2. Very weak signals of sulphur and fluorine indicate the trace amounts of the dissolving salt ($NaSO_3CF_3$). In Figure 11b, the characterization signals

accord with oxygen, sodium, calcium, manganese and nickel elements with a relative atomic composition of about 54%, 17%, 12%, 12% and 4%, respectively. After excluding the oxygen content of the catalyst, the mole ratio of the oxygen to sodium is about 1:1, which offer further evidence of the existence of Na_2O_2. The Ca, Mn, and Ni signals are from the $CaMnO_3$ catalyst and the nickel foam current collector.

References:

[s1] Reller, A.; Thomas, J. M.; Jefferson, D. A.; Uppal, M. K. *Proc. R. Soc. Lond. A* **1984**, *394*, 223.

[s2] Han, X. P.; Zhang, T. R.; Du, J.; Cheng, F. Y.; Chen, J. *Chem. Sci.* **2013**, *4*, 368.